Clinical Neurophysiology 127 (2016) 2308–2316

Contents lists available at ScienceDirect

Clinical Neurophysiology

journal homepage: www.elsevier.com/locate/clinph

High-resolution MEG source imaging approach to accurately localize Broca's area in patients with brain tumor or epilepsy

Charles W. Huang [a], Ming-Xiong Huang [b,c,*], Zhengwei Ji [b], Ashley Robb Swan [c], Anne Marie Angeles [c], Tao Song [b], Jeffrey W. Huang [d], Roland R. Lee [b,c]

[a] Department of Bioengineering, University of California, San Diego, San Diego, CA, USA
[b] Department of Radiology, University of California, San Diego, San Diego, CA, USA
[c] Research Services, VA San Diego Healthcare System, San Diego, CA, USA
[d] Westview High School, San Diego, CA, USA

ARTICLE INFO

Article history:
Accepted 9 February 2016
Available online 17 February 2016

Keywords:
Broca
Wernicke
Expressive language
Receptive language
Object-naming task

HIGHLIGHTS

- Magnetoencephalography (MEG) provides high localization accuracy for Broca's and Wernicke's areas.
- MEG reveals time latency differences between Wernicke's and Broca's areas.
- MEG assesses dominance in Broca's area in patients with brain tumor or epilepsy.

ABSTRACT

Objective: Localizing expressive language function has been challenging using the conventional magnetoencephalography (MEG) source modeling methods. The present MEG study presents a new accurate and precise approach in localizing the language areas using a high-resolution MEG source imaging method.
Methods: In 32 patients with brain tumors and/or epilepsies, an object-naming task was used to evoke MEG responses. Our Fast-VESTAL source imaging method was then applied to the MEG data in order to localize the brain areas evoked by the object-naming task.
Results: The Fast-VESTAL results showed that Broca's area was accurately localized to the pars opercularis (BA 44) and/or the pars triangularis (BA 45) in all patients. Fast-VESTAL also accurately localized Wernicke's area to the posterior aspect of the superior temporal gyri in BA 22, as well as several additional brain areas. Furthermore, we found that the latency of the main peak of the response in Wernicke's area was significantly earlier than that of Broca's area.
Conclusion: In all patients, Fast-VESTAL analysis established accurate and precise localizations of Broca's area, as well as other language areas. The responses in Wernicke's area were also shown to significantly precede those of Broca's area.
Significance: The present study demonstrates that using Fast-VESTAL, MEG can serve as an accurate and reliable functional imaging tool for presurgical mapping of language functions in patients with brain tumors and/or epilepsies.

1. Introduction

Currently, magnetoencephalography (MEG) has been routinely used as a noninvasive presurgical functional mapping tool in patients with brain tumors and/or epilepsies. This is mainly due to the better localization accuracy (in several millimeters for cortical areas; Huang et al., 2006; Leahy et al., 1998; Niranjan et al., 2013), compared to scalp electroencephalography (EEG), and higher temporal resolution (in 1 ms) of MEG, compared to several other commonly known functional mapping techniques, such as functional magnetic resonance imaging (fMRI, in sec) and positron emission topography (PET, in min). MEG has been proven to be highly valuable in localizing activity in the somatosensory cortex (Huang et al., 2000, 2005; Niranjan et al., 2013; Schiffbauer et al., 2001, 2003), motor cortex (Bourguignon et al., 2013; Huang

* Corresponding author at: Radiology Imaging Laboratory, University of California, San Diego, 3510 Dunhill Street, San Diego, CA 92121, USA. Tel.: +1 858 534 1254; fax: +1 858 552 7404.
E-mail address: mxhuang@ucsd.edu (M.-X. Huang).

http://dx.doi.org/10.1016/j.clinph.2016.02.007
1388-2457/Published by Elsevier Ireland Ltd. on behalf of International Federation of Clinical Neurophysiology.

et al., 2004; Pang et al., 2008; Schiffbauer et al., 2001), auditory cortex (Chen et al., 2013; Edgar et al., 2006, 2008; Huang et al., 2003; Nakasato et al., 1997), and receptive language areas (i.e., Wernicke's area) (Billingsley-Marshall et al., 2007; Papanicolaou et al., 1999, 2004, 2005, 2006). Yet, it has been previously challenging to localize expressive language function (i.e., the activity in Broca's area) using MEG.

In presurgical planning, evaluation of a patient's language function has become an important procedure that requires high accuracy and reliability. In general, presurgical language mapping approaches can be divided into three categories with different spatial scales: (1) *the large-scale language lateralization* approach that addresses the question whether the left or right hemisphere is the language-dominant hemisphere, without assessing the exact location of specific anatomical areas; (2) *the language localization* approach that reveals the voxels in specific anatomical areas controlling the language function; and (3) the *ROI-based small-scale lateralization* approach that assesses the anatomical areas in the left or right hemisphere controlling the language function. In these approaches, signals from voxels within the specific anatomical areas or regions of interest (ROIs) are usually summed up, and then the summed signals are used to assess lateralization (Hirata et al., 2004).The present study deals with voxel-wise language localization and ROI-based small-scale language lateralization.

The large-scale language lateralization evaluation has been traditionally administered through the Wada Test (Wada and Rasmussen, 1960), more formally known as the intracarotid sodium amobarbital procedure. However, a major limitation of the Wada Test is that it does not localize language areas, whereas for surgical planning, ROI-based small-scale language lateralization and language localization are often essential. Thus, noninvasive functional neuroimaging has become an important component of language mapping in clinical settings. FMRI, in particular, is a neuroimaging method that monitors change in blood oxygenation level-dependent (BOLD) contrast imaging to measure the corresponding change in neural activity. Yet, for patients, the limitations of fMRI include the possibility of claustrophobia, loud high-pitched noises caused by the Lorentz forces induced in the gradient coils, and the intolerance of head movement during scans. Moreover, the fMRI BOLD effect may be disturbed by pathological vascularization in the tumor that prevents a local increase of blood flow, thus resulting in lower BOLD contrast (Grummich et al., 2006; Holodny et al., 1999, 2000; Roux et al., 2003; Schreiber et al., 2000). By contrast, MEG provides direct measurements of neural activity and is insensitive to the abnormal blood flow-related artifacts in tumors. MEG recordings are conducted in a quiet environment, and the ability to perform head motion tracking and correction in Elekta/Neuromag MEG machines (Taulu et al., 2004a; Taulu and Simola, 2006) also enhances the potential of MEG as a clinical tool for language localization and ROI-based small-scale language lateralization.

In the MEG literature, studies of expressive language localization (i.e., Broca's area) have been limited. Salmelin and colleagues performed one of the first MEG studies to examine responses in Broca's area using a naming task and a dipole-fitting analysis (Salmelin et al., 1994). However, in their study, large discrepancies in the dipole locations of Broca's area may limit the application of dipole fitting during presurgical mapping in a clinical setting.

Using picture verb generation and word verb generation tasks, Pang and colleagues examined the MEG and fMRI responses in 10 healthy subjects (Pang et al., 2011). Beamformer (Gross et al., 2001; Gross and Ioannides, 1999; Robinson and Vrba, 1999; Sekihara et al., 2001; Van Veen et al., 1997) was used in that study for MEG source localization. They found 79.6% overlap of voxels activated by both MEG and fMRI for picture verb generation and 50.2% overlap for word verb generation. However, our close examination of the figures in the work from Pang and colleagues suggests large discrepancies in the exact cortical representation of Broca's area responses between fMRI and MEG. Many of the MEG frontal lobe hot spots reported in their study appear to be outside of the typical Broca's area including pars opercularis (Brodmann Area or BA 44) and pars triangularis (BA 45). Wernicke's responses were not examined in the above study by Pang and colleagues (Pang et al., 2011).

In addition, using the beamformer analysis, Hirata and colleagues examined the beta and gamma band desynchronization during a silent reading task in presurgical patients. Based on MEG activity in inferior frontal areas as part of an ROI-based small-scale lateralization approach, they reported that in 95% of the cases, the MEG small-scale lateralization results were congruent with the result of the Wada Test (Hirata et al., 2004). In addition to the inferior frontal areas, activity from other brain areas such as middle frontal lobe, temporal–occipital lobe, and angular/lateral occipital areas was also reported in that study (Hirata et al., 2004). However, the spatial resolution of the source images from their approach appears to be limited, and the sequence of activation between the activity in inferior frontal activity and other brain regions was not presented.

In another MEG study using beamformer analysis, Bober and colleagues examine the MEG responses evoked by a silent reading and a silent naming task in eight healthy subjects and seven patients with brain tumors (Kober et al., 2001). They reported localization of both Wernicke's and Broca's areas. However, our examination of the figures in that study showed that the inferior frontal sources obtained from their beamformer analysis were actually from the precentral gyri as part of the motor cortex, again not the typical Broca's area (i.e., pars opercularis/BA 44 and pars triangularis/BA 45), although some studies included the inferior aspect of the precentral gyrus as part of Broca's area (Price, 2000). In a separate study of 172 patients with brain tumors from the same laboratory, Kober, Grummich, and their colleagues used sequential dipole fits (4D-Neuroimaging proprietary software) and beamformer analysis to localize the MEG responses in Broca's and Wernicke's areas evoked by several language tasks (Grummich et al., 2006). Many of these patients were also examined using fMRI. Their findings report congruence between fMRI and MEG in 77% of the localizations of language areas. They also reported Broca's activity that was localized to the frontal operculum and the ventral premotor cortex using MEG. The discrepancies in MEG localization of Broca's area in the above studies suggest that further studies are warranted for addressing MEG's accuracy in localizing the expressive language function.

We believe that the discrepancies in MEG's localization of Broca's area from the above studies were at least in part due to the dipole fitting and beamformer techniques. In the current study, we assessed the accuracy of using our Fast-VESTAL MEG source imaging method in localizing expressive language function, especially Broca's area using an object-naming task. Our recent development of the high-resolution MEG source imaging method, Fast-VESTAL, allows for a voxel-wise whole-brain source imaging of human brain function in a more advanced way than the traditional methods (e.g., dipole fits, minimum L2 norm approaches, and beamforming; Huang et al., 2014a). Advantages of Fast-VESTAL over the standard MEG methods include its ability to (1) localize multiple correlated sources without distorting activity, (2) faithfully recover source time courses, and (3) generate accurate statistical maps of source images without signal leakage to other brain areas. Fast-VESTAL and its processor, VESTAL, have been successfully applied in analyzing resting-state as well as evoked MEG signals(Chen et al., 2013; Diwakar et al., 2015; Huang et al., 2006, 2009, 2010, 2012, 2014a,b,c; Robb et al., 2015).

The primary goals of our present MEG study are as follows: (1) Use a single-subject basis analysis to examine Fast-VESTAL's voxel-wise localizations of Broca's area during an object-naming task in individual patients with brain tumors and/or epilepsies. (2) Examine the ROI-based small-scale language lateralization and language dominance using an asymmetry index for Broca's responses. In this type of ROI-based group analysis, the source activity from pars opercularis (BA 44) and pars triangularis (BA 45) was summed up. (3) Use a voxel-wise group-analysis approach to examine the common features across patients of the brain activity localizations inside as well as outside Broca's area. In this approach, the MEG activity of individual patients from the object-naming task was co-registered to the MNI-152 brain atlas. (4) Examine the latency differences between Broca's and Wernicke's responses. In the present study, we adopt the typical definition of Broca's area to include the pars opercularis (BA 44) and pars triangularis (BA 45) and the typical definition of Wernicke's area in BA 22 to be located in the posterior section of the superior temporal gyrus (STG).

2. Materials and methods

2.1. Clinical cases and MEG object-naming task

De-identified MEG object-naming data from 35 clinical patients obtained from the UCSD clinical MEG database were selected for this study. Among these patients, two were removed from the actual study due to severe artifacts in their MEG data caused by metal objects, which could not be removed by our software (see MEG artifact removal procedure later). An additional patient was removed from the study because this patient with epilepsy had highly frequent interictal spike discharges from the pars opercularis and pars triangularis, which may have contaminated the MEG responses evoked by object-naming task. The MEG data from the remaining 32 patients were used in this study.

Among these 32 patients, 22 were men and 10 women; the mean value and standard deviation (SD) for age were 41.2 years and 18.2, respectively. Among these patients, 21 patients had brain tumors (19 with left frontal/temporal lobe tumors and two with right frontal tumors), seven epilepsies, and four both epilepsies and left frontal/temporal lobe tumors. The MEG data were collected under our standard clinical protocol for presurgical functional mapping in patients with brain tumors and/or epilepsies. Among these patients, 27 were right-handed and five left-handed.

The stimuli used in the MEG object picture-naming task were taken from the UCSD Center for Research in Language-International Picture-Naming Project (CRL-IPNP) database (http://crl.ucsd.edu/experiments/ipnp/) (Bates et al., 2003; Szekely et al., 2005), which contains 520 black-and-white two-dimensional line drawings representing different objects. These items have been tested in healthy and patient populations across seven different international sites and languages. Presentation software (Neurobehavioral systems) was used to display these pictures on a screen via a Panasonic DLP projector (PT-D7700U). The stimuli were displayed with inter-stimulus intervals of 2 s in a random order and without repeats. The patient was then instructed to name each object silently as soon as the object was displayed on screen.

2.2. MEG data acquisition and signal preprocessing to remove artifacts

MEG responses to the object-naming stimuli were collected at the UCSD MEG Center using the VectorView™ whole-head MEG system (Elekta-Neuromag, Helsinki, Finland) with 306 MEG channels. Patients sat inside a multilayer magnetically shielded room (IMEDCO-AG) (Cohen et al., 2002). Precautions were taken to ensure head stability; foam wedges were inserted between the participant's head and the inside of the unit, and a Velcro strap was placed under the participant's chin and anchored in superior and posterior axes. Head movement across different sessions was about 2–3 mm. MEG data were then sampled at 1000 Hz and run through a high-pass filter with a 0.1-Hz cutoff, a low-pass filter with a 300-Hz cutoff, and a notch filter (58–62 Hz) to remove 60-Hz power-line noise. Eye blinks, eye movements, and heart signals were recorded simultaneously with the MEG data. Maxfilter, also known as signal space separation (Song et al., 2008; Taulu et al., 2004a,b), was used to remove external interferences from the raw MEG data. A total of 100 artifact-free responses were then averaged with respect to the stimulus trigger to increase the signal-to-noise ratio (SNR).

2.3. Structural MRI, MEG–MRI registration, and BEM forward calculation

Structural T1-weighted MRIs of the patients were used to co-register the MEG source imaging as well as to construct realistic boundary element method (BEM) head models for the MEG forward calculations. The MRI data were obtained from a variety of MRI scanners (GE, Siemens, and Philips) at either 1.5T or 3T field strength. All T1-weighted MRIs were examined by Dr. Roland Lee (neuroradiologist) to ensure that the imaging resolution, contrast, and SNR meet the requirements of the MEG. If the preexisting MRI did not meet the MEG requirements, a new T1-weighted MRI was collected using the General Electric 1.5T Excite MRI scanner, in the same building as the MEG scanner. The acquisition contains a standard high-resolution anatomical volume with a resolution of $0.94 \times 0.94 \times 1.2\ mm^3$ using a T1-weighted 3D-IR-FSPGR pulse sequence.

To co-register the MEG with the MRI coordinate systems, three anatomical landmarks (i.e., left and right preauricular points, and nasion) were measured for each participant using the Probe Position Identification system (Polhemus, VT, USA). Using MRILAB (Elekta/Neuromag) for identifying the same three points on the participant's MRIs, a transformation matrix involving both rotation and translation between the MEG and MR coordinate systems was established. In order to increase the reliability of the MEG–MR co-registration, approximately 100 points on the scalp were digitized with the Polhemus system, in addition to the three landmarks, and those points were co-registered onto the scalp surface of the MR images. The T1-weighted images were also used to extract the brain volume and innermost skull surface (SEGLAB software developed by Elekta/Neuromag). A realistic BEM head model was used for MEG forward calculation (Huang et al., 2007; Mosher et al., 1999). The BEM mesh was constructed by tessellating the inner skull surface from the T1-weighted MRI into ~6000 triangular elements with ~5-mm size. A cubic source grid with 5-mm size was used for calculating the MEG gain (i.e., lead-field) matrix, which leads to a grid with ~10,000 nodes covering the whole brain.

2.4. MEG source magnitude imaging with Fast-VESTAL

Voxel-wise MEG source magnitude images were obtained using our recent high-resolution Fast-VESTAL MEG source imaging method (Huang et al., 2014a). Waveforms from all 306 sensors including 204 planar gradiometers and 102 magnetometers were used in the analysis. In this approach, we first calculated the sensor–waveform covariance matrix for the 200–1000 ms poststimulus interval and used the −200 to 0 ms baseline interval for estimating baseline noises and DC corrections. A low-pass filter with a cutoff frequency of 50 Hz was used when calculating the sensor–waveform covariance matrix. Using such a sensor–waveform covariance matrix, MEG source magnitude images covering the whole brain were obtained following an updated version of

our previously published Fast-VESTAL algorithm (Huang et al., 2014a). Fast-VESTAL is a spatiotemporal L1 minimum norm solution applying L1 constraints to fit the sensor waveforms. Extensive computer simulations with white and brain noises, at a variety of noise levels, have been used in validating the Fast-VESTAL approach (Huang et al., 2014a). For further validations, Fast-VESTAL has been applied to the resting state as well as evoked MEG data in humans, and the results were highly consistent with established knowledge of neurophysiology (Huang et al., 2014a). The change of this updated version from its original Fast-VESTAL formulation involves the adoption of a second-order cone programming strategy (SOCP) for the L1 minimum norm solver (see Supplementary Appendix A for details).

2.5. Single-subject-based Voxel-wise MEG source magnitude images for language localization

As the anatomical areas BA 44 and 45, commonly considered as Broca's area, are sizable brain areas, high-resolution MEG language location is essential for presurgical planning. In the present study, we used voxel-wise MEG localization with Fast-VESTAL to provide more precise information about the language localization within these sizable anatomical areas in a single-subject-based analysis. Such voxel-wise high-resolution MEG source magnitude images have to be provided to the neurosurgeons in a single-subject basis.

For each patient's Fast-VESTAL source magnitude imaging data, voxel-wise *F*-tests were used to assess the variances between the poststimulus 200–1000 ms interval over the prestimulus interval of −200 to 0 ms for each grid node. The voxel-wise *F*-value maps for the Fast-VESTAL solution were constructed for the ~10,000 grid nodes. False discovery rate (FDR) (Benjamini and Hochberg, 1995) corrected for multiple comparisons (corrected $p = 0.01$) was employed. This procedure was the same as described in our previous publication (Huang et al., 2014a). The emphasis here is to examine Fast-VESTAL's voxel-wise localization of Broca's area in each patient.

2.6. ROI-based small-scale MEG language lateralization for Broca's area

This subsection describes the procedure for examining the small-scale language lateralization and language dominance using the asymmetry index for Broca's responses. In ROI-based small-scale lateralization, it is important to integrate functional imaging information from MEG with the previously established knowledge of neurophysiology and anatomy. When mapping the expressive language, many statistically significant sources often light up during the task. Previous knowledge of neurophysiology and anatomy can help us select the statistically significant sources within the pars opercularis/BA 44 and pars triangularis/BA 45 for expressive language function. However, the knowledge of neurophysiology and anatomy cannot help in determining whether left or right BA 44 and 45 are responsible for expressive language. It is worth noting that we move beyond large-scale language lateralization and into ROI-based small-scale lateralization. We want to know not only which hemisphere controls the expressive language, but also specifically if the left BA 44 and 45 ROIs are for language expression. For the purposes of the ROI-based small-scale lateralization, we sum up all activities within the mask covering the BA 44 and 45 areas for the group analysis of language dominance.

Specifically, the voxel-wise Fast-VESTAL root mean square (RMS) values for the 200–1000 ms poststimulus interval were first spatially co-registered to an MNI-152 brain–atlas template using a linear affine transformation via FLIRT program in FSL software package (www.fmrib.ox.ac.uk/fsl/). Next, in the MNI-152 coordinates, an ROI-based mask was constructed, which contains the pars opercularis (Brodmann Area or BA 44) and pars triangularis (BA 45) in the left and right inferior frontal gyri, expanding to the frontal operculum cortex to account for MEG's less sensitivity in depth (see Fig. 1). Visual inspections were performed to ensure that the ROI-based mask accurately covered the pars opercularis (BA 44) and pars triangularis (BA 45). Such an ROI-based mask was applied to the voxel-wise Fast-VESTAL RMS source images, and all activity within the mask was summed up for left and right hemispheres, respectively (i.e., L_{sum} and R_{sum}). The standard asymmetry index was calculated using Eq. (1):

$$\text{Asym} = \frac{L_{sum} - R_{sum}}{L_{sum} + R_{sum}} \times 100\% \quad (1)$$

The above approach was similar to a previous ROI-based lateralization approach by Hirata and colleagues. However, the definition of asymmetry index in Eq. (1) is different from the one used by Hirata and colleagues (Hirata et al., 2004) by a factor of two.

2.7. Voxel-wise group statistical analysis on brain area evoked by object-naming task

Next, voxel-wise group statistical analysis was performed to reveal the common brain areas evoked by the MEG object-naming task. The voxel-wise MEG source magnitude imaging volumes obtained with Fast-VESTAL covering the whole brain from all patients were first spatially co-registered to the MNI-152 brain–atlas template using the FLIRT program and then spatially smoothed using a Gaussian kernel with 5-mm full width half maximum (FWHM). For each voxel in the MNI space, the MEG source magnitude data were run through a logarithmic transformation. For each voxel of the brain volume in the MNI space, a paired *t*-test was performed to assess the differences in root mean square (RMS) values between the 200 and 1000-ms poststimulus intervals and −200 to 0 ms prestimulus intervals. A standard cluster analysis was performed for the *t*-value maps to control for family-wise errors at a corrected $p < 0.01$ level, using "3dFWHMx" and "3dClustSim" functions in AFNI (http://afni.nimh.nih.gov). A mask that contains the statistically significant clusters was created and then applied to the *t*-value maps to create group statistical maps for the MEG source magnitude images. The emphasis here is to examine all common brain areas (not limited to Broca's area) evoked by the object-naming task.

3. Results

3.1. Results for single subject-based Voxel-wise MEG language localization

First, MEG activity evoked by the object-naming task in individual patients was examined on a single-subject basis. Fig. 2 shows axial cuts of the MEG responses in Broca's area (green arrows) from

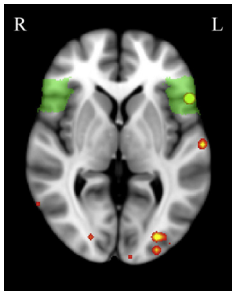

Fig. 1. Applying a mask (green color) used in an ROI-based small-scale lateralization measurement to calculate asymmetry of the MEG response in Broca's area.

10 representative patients obtained using Fast-VESTAL. In each subject, a voxel-wise *F*-test was used to assess the statistical significance of the RMS values for each grid node between the 200 and 1000-ms poststimulus interval and −200 to 0 ms prestimulus baseline. False discovery rate (FDR) corrected for multiple comparisons (corrected $p = 0.01$) was employed, as described in the previous publication (Huang et al., 2014a). Among these 10 patients, eight showed markedly stronger activity in left Broca's area, one showed similar responses in bilateral Broca's area, and one showed markedly stronger activity in right Broca's area. In several subjects, the responses in the left hemispheric Wernicke's area are also visible in the axial cuts; in addition, activity from visual cortices was also commonly visible.

Among the 32 patients, two right-handed patients had large left frontal lobe tumors that severely distorted the left pars opercularis (Brodmann Area or BA 44) and pars triangularis (BA 45) in the inferior frontal gyrus with Broca's area (Fig. 3). In these two patients, the MEG responses were still accurately localized to the highly distorted pars opercularis or pars triangularis by Fast-VESTAL (see three views in Fig. 3). However, the structural distortions were too severe to correctly register their MRI data to the standard MNI-152 atlas using the linear affine transformation (see Section 2). Specifically, after the affine transformation, their MRI images failed our visual inspections due to large mismatches to the MNI-152 atlas in the pars opercularis and pars triangularis areas. Thus, the MEG data from these two patients were excluded from further group analyses in the present study.

3.2. Results for ROI-based small-scale MEG language lateralization for Broca's area

In the remaining 30 patients, their MRI data were successfully registered to the MNI-152 atlas, and their MEG Fast-VESTAL source images were used in further group analysis. In order to provide a

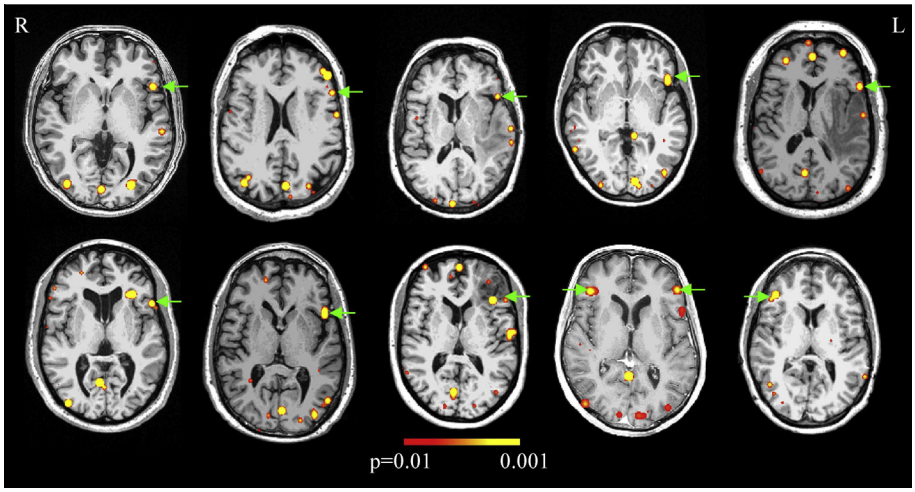

Fig. 2. Single-subject-based MEG localization of Broca's area (green arrows) in ten representative patients during object-naming task using Fast-VESTAL. In each subject, an *F*-test was used to assess the statistical significance of the source magnitude (RMS value) between a 200 and 1000-ms poststimulus interval and prestimulus baseline. The MEG data of subjects were also used in a group analysis.

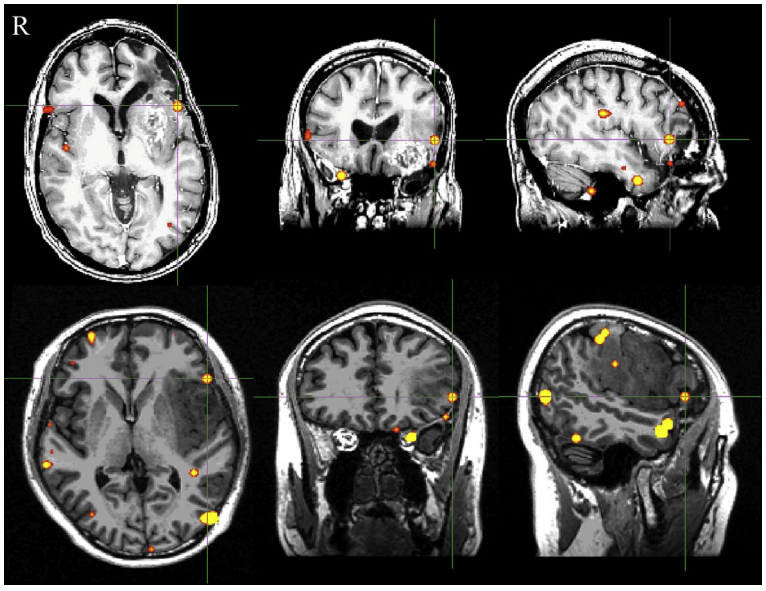

Fig. 3. Single-subject-based MEG localization of Broca's area (green crossing hairs) in two subjects with large left frontal lobe tumors during object-naming task using Fast-VESTAL. The settings of the statistical significance in this figure are the same as in Fig. 2. The MEG data from these two patients with large tumors were not used in further group analyses as the linear affine transformation failed to correctly register the MRIs of these two patients to the MNI-152 atlas.

quantitative measure of the ROI-based small-scale language lateralization/dominance, the asymmetry index (Eq. (1)) of the MEG activity from Broca's area was calculated for these 30 patients. The procedure has been described in the Materials and Methods section, after applying the ROI-based mask (see Fig. 1). Fig. 4 plots the histogram of the asymmetry index. Empirically, the entire asymmetry scale was uniformly divided into three regions: dominance in left Broca's area (33.3–100.0%), dominance in right Broca's area (−100.0% to −33.3%), and bilateral Broca representation (−33.3% to 33.3%). Among these 30 patients, 23 (or 76.7%) were in the left Broca-dominant group, four (or 13.3%) in the bilateral group, and three (or 10.0%) in the right Broca-dominant group. We also found that two patients were left-handed among the three patients with right Broca dominance. There was one left-handed patient among the four patients with bilateral Broca representation.

3.3. Results of Voxel-wise group analysis on brain areas evoked by object-naming task

Next, voxel-wise group statistical analysis was performed to reveal the common brain areas evoked by the MEG object-naming task (see Section 2). Fig. 5 shows the significant MEG responses during the 200–1000 ms poststimulus interval and prestimulus baseline in the 30 presurgical patients. In this figure, *t*-value maps of the MEG source magnitude images within the cluster-analysis mask that was associated with corrected $p < 0.01$ are displayed (see Section 2). Significant responses were shown in language network including the left Broca's and left Wernicke's areas. Significant responses were also shown in the parietal attention network including the bilateral supramarginal gyri and bilateral angular gyri. In addition, both primary visual and other dorsal and ventral visual areas showed strong responses. Furthermore, the bilateral ventral temporal and temporal pole areas showed strong responses as well. Finally, the ventromedial prefrontal cortex and bilateral frontal pole areas showed strong responses. It appears that Broca's area and Wernicke's area are the two brain areas with strong scenarios of lateralization, as both have markedly stronger left hemisphere responses than those of the right hemisphere.

The peak latencies of the MEG activity in Wernicke's and Broca's areas were analyzed. Fig. 6 plots the peak latency of these areas in individual patients. The peak latency was obtained from the source time course for the voxel with highest activity (for the 200–1000 ms poststimulus interval) within Broca's and Wernicke's areas. All 30 patients showed a main peak for Wernicke's source with a latency of 315 ± 80.6 ms (mean ± SD). All 30 patients showed a main peak for Broca's source with a latency of 643.9 ± 188.1 ms. The main peak latency of Wernicke's source is significantly earlier than that of Broca's source ($t = 8.8$, $p < 10^{-11}$, $df = 58$). In addition, we found an earlier and weaker peak in the source time courses of Broca's area in 15 (i.e., 50%) patients, with a peak latency of 282.9 ± 14.8 ms. However, we found no statistical difference in latency between this early peak in Broca's source and main peak in Wernicke's source ($p > 0.2$).

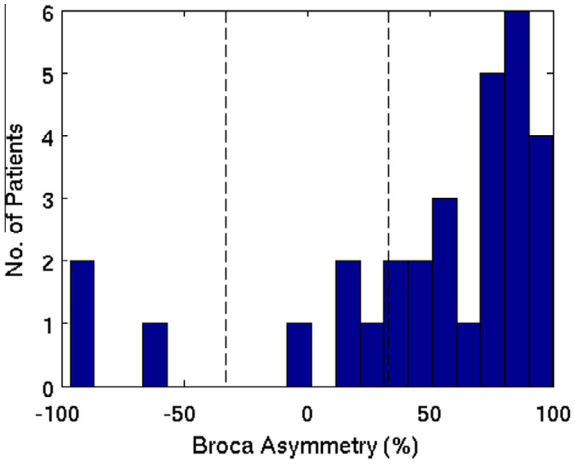

Fig. 4. ROI-based small-scale language lateralization using asymmetry index of MEG responses from Broca's area during object-naming task in 30 presurgical patients. The two dashed lines divide the subjects into three groups: left Broca-dominant (33.3–100.0%), right Broca-dominant (−100.0% to −33.3%), and bilateral (−33.3 to 33.3%) groups.

3.4. Computational costs

The computational cost of Fast-VESTAL analysis is rather low. All Fast-VESTAL programs were developed in MATLAB™ (MathWorks, Natick, MA, USA), and all analyses were done on a Dell Precision 7500 Workstation with Dual Intel Xeon X5550 Processors (each with 8 M Cache, 2.67 GHz, and 6.40 GT/s QPI) and with 24 GB system RAM. Although Fast-VESTAL is inherently a good candidate for parallel processing, no parallel processing was performed in the present study. For a grid with ~10,000 nodes covering the whole brain, the CPU time was about 108 s for analyzing a typical MEG dataset using Fast-VESTAL.

4. Discussion

While language-related functions, namely speech production and perception, were among the first localized in the brain, much research and advancement in neuroimaging technology has expanded the understanding of the neural networks underlying language-related functions. Although the networks involved in language-related functions are complex, the "classical model" of language organization, popularized in the 19th century by Wernicke and Geshwind, suggests that expressive language functions can be localized to a frontal area of the brain named after Broca. This model also proposes a posterior area of the brain, more responsible for receptive language functions, named after Wernicke. However, this classical model has some limitations: (1) It does not specifically detail the cortical areas that make up Broca's and Wernicke's areas, and (2) it fails to account for the complex connections between the sensory and association areas. The present MEG study greatly contributed, along with many fMRI and PET studies (see review in (Price, 2000)), in assessing the former limitations of the classical model.

In a single subject-based approach, using Fast-VESTAL, the high-resolution MEG source imaging technique, we were able to accurately localize Broca's and Wernicke's areas in 32 patients with brain tumors and/or epilepsies during the object-naming task. Broca's responses in the present study were all localized to the typical Broca's area in the pars opercularis (BA 44) and/or pars triangularis (BA 45) in the inferior frontal gyri, mainly to the ventral aspect of the pars opercularis and/or pars triangularis. Even in the two cases wherein the inferior frontal lobe brain structures were highly distorted by brain tumors, Fast-VESTAL still accurately localized the MEG responses to the highly distorted pars opercularis or pars triangularis (Fig. 3). Thus, the exclusion of these two cases from the rest of the group analyses was not a limitation of the Fast-VESTAL but of the linear affine transformation of the MRI data.

The result of the present study shows substantial improvement in spatial accuracy and resolution for localizing the responses of Broca's area over the previous MEG studies (Grummich et al., 2006; Hirata et al., 2004; Kober et al., 2001; Pang et al., 2011;

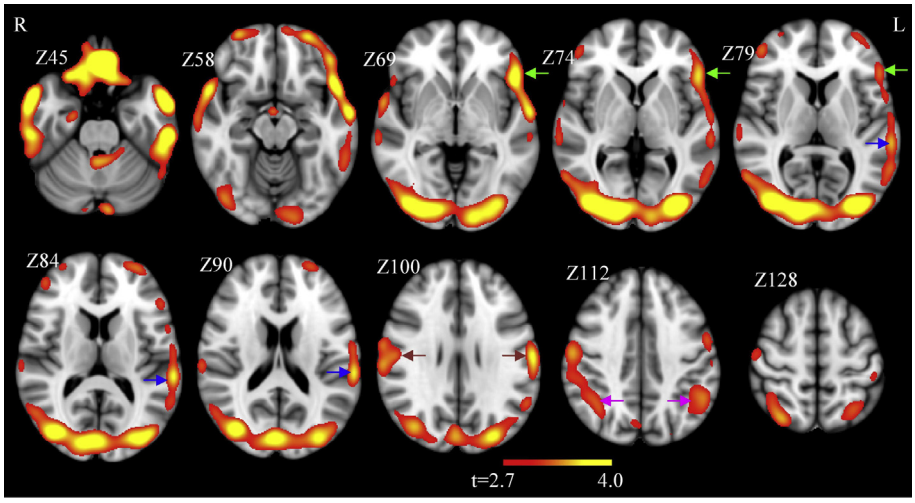

Fig. 5. Voxel-wise significant MEG responses evoked by object-naming task, during 200–1000 ms poststimulus interval versus prestimulus baseline in 30 presurgical patients. Arrows indicate the responses in left hemispheric Broca's area (green arrows), left hemispheric Wernicke's area (blue arrows), bilateral supramarginal gyri (brown arrows), and bilateral angular gyri (magenta arrows). The corrected *p* threshold was set at 0.01 in cluster analysis to correct for family-wise errors. *Z* coordinate in MNI-152 atlas was shown for each axial slice.

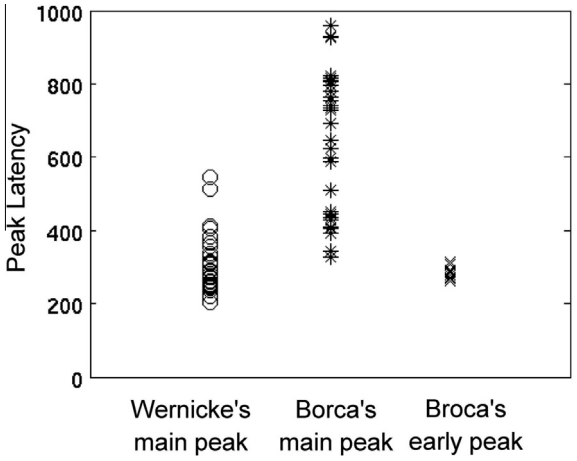

Fig. 6. Peak latency of source time courses in Wernicke's and Broca's areas. Some patients also showed an earlier peak in Broca's area.

Salmelin et al., 1994). We believe that in the previous MEG studies, discrepancies in the localization of Broca's area were at least in part due to the beamformer techniques used. Beamformer assumes that different brain sources are uncorrelated, and this assumption may not be strictly valid for activities evoked by language tasks when many brain areas are potentially firing synchronously. In addition, Fast-VESTAL showed improvements in localization accuracy and success rate over the conventional single sequential dipole fitting approach which only successfully localized the expressive and receptive language cortex 50–70% of the time (Grummich et al., 2006; Rezaie et al., 2014).

In the present study, we found that 76.7% patients were in the left Broca-dominant group, 13.3% were in the bilateral group, and 10.0% were in the right Broca-dominant group. These values are similar to the 81% left dominance, 16% bilateral, and 3% right dominance in a previous MEG study conducted by Grummich and colleagues (Grummich et al., 2006). They are also consistent with the 80% left dominance and 20% right dominance in another MEG study by Hirata and colleagues (Hirata et al., 2004). The percentages of left hemisphere dominance in these three MEG studies, including ours, appear to be <93% of left hemisphere speech dominance in the overall population, as per the Wada Test (Wada and Rasmussen, 1960). We believe that the difference was due to the fact that the majority of our 30 patients had tumors in the left frontal and/or temporal lobes, which differed from the general population of the Wada Test study (Wada and Rasmussen, 1960). Functional reorganization to the right hemisphere during the year of the tumor development cannot be excluded as a contributing factor for the patients in our present study.

Similarly, in the present study, the latency of the main peak of Wernicke's activity (i.e., 315 ± 80.6 ms) was significantly earlier than that of the main peak of Broca's activity (i.e., 643.9 ± 188.1 ms). This result is consistent with findings in previous MEG studies with similar tasks that showed Wernicke's peak activity at ~300 ms and Broca's peak activity at ~600 ms in some patients (Grummich et al., 2006; Kober et al., 2001; Salmelin et al., 1994). However, our study provides the first statistically significant finding in those main peak latencies between the receptive and expressive language areas. In 50% of our patients, we also found a weaker and earlier peak at 282.9 ± 14.8 ms in Broca's source time courses, which did not statistically differ from the main peak latency of Wernicke's source. This weaker and earlier Broca's peak was reported previously (Grummich et al., 2006) in a subset of patients. The exact function of such a weaker and earlier peak from Broca's area is unclear; however, we believe that this earlier Broca's activity may be related to language priming (Misiurski et al., 2005; Sakai et al., 2002; Silkes and Rogers, 2012).

Besides Broca's, Wernicke's, and visual areas, we also found significant responses in the bilateral supramarginal gyri and bilateral angular gyri. These visual areas provide essential sensory inputs in processing visual stimuli. In the present study, the supramarginal gyrus and angular gyrus areas did not show strong lateralization compared to Broca's and Wernicke's area. In the previous fMRI studies (see review in (Price, 2000)), the angular gyrus is known to be part of a distributed semantic system that can be accessed by stimuli of objects and faces as well as speech. Conversely, the supramarginal gyrus was shown to be involved in processing phonological information (Demonet et al., 1994; Devlin et al., 2003; Mummery et al., 1998; Price et al., 1997) or due to automatically computing the sound of words (Stoeckel et al., 2009).

In the present study, we believe that a major contributor for obtaining good localization of the activity in Broca's area was the application of our Fast-VESTAL algorithm. Fast-VESTAL differs from

some conventional L1 minimum norm solutions (e.g., MCE in Elekta/Neuromag software package) or L2 minimum norm solutions (e.g., the ones implemented in BrainStorm software package) in several ways. MCE (Uutela et al., 1999) is a L1 minimum norm solution with a least-squares fit to the sensor waveform signal (i.e., L2 constraints). Here, the basic functions are the lead-field (i.e., gain) matrix or the vector spherical harmonic functions when sensor waveforms are run through MaxFilter (Taulu et al., 2004a; Taulu and Simola, 2006). Like other conventional L1 minimum norm solutions, the reconstructed source time-courses from MCE suffer from "spiky" or discontinuous features. In our standard VESTAL approach (Huang et al., 2006), we first introduced a spatiotemporal projection in an L1 minimum norm solution, with L1 constraints in fitting the sensor waveforms, which effectively solved this major problem associated with the "spiky" or discontinuous source time courses.

However, one limitation of the standard VESTAL and MCE has been the relatively high computational costs when the number of time samples is large. This is because in the standard VESTAL, the large number of L1 minimum norm solutions, with L1 constraints for fitting the sensor waveforms, need to be solved time point by time point. By contrast, in the present study, we used Fast-VESTAL (Huang et al., 2014a), which requires a much lower computational cost. Like in the standard VESTAL (Huang et al., 2006), Fast-VESTAL also adopts the spatiotemporal projection using the temporal modes in the sensor waveforms. However, unlike the standard VESTAL, Fast-VESTAL obtains source magnitude images for a smaller number of spatial modes of the sensor waveforms, which in turn results from the spatiotemporal projections (see Eq. (A4) in the Supplementary Appendix A). Specifically, Fast-VESTAL obtains the optimally weighted L1 minimum norm solutions of source magnitude images with L1 constraints applied when fitting the spatial modes of the sensor waveforms ((Huang et al., 2014a), also see the Supplementary Appendix A). The optimal weighting in Fast-VESTAL is crucial for obtaining the accurate localizations in depths, e.g., subcortical sources (US Patent Provisional Application Attorney Docket No.: 009062-8264.US00). This feature has been supported by the resting-state MEG study on post-traumatic stress disorder (PTSD) wherein deep brain activity from ventral–medial frontal lobe, insular cortex, amygdala, and hippocampus were reliably localized (Huang et al., 2014c).

However, the variety of approaches in the category of L2 minimum norm solutions with L2 constrains implemented by BrainStorm (Tadel et al., 2011) was based on dSPM (Dale et al., 2000) and sLORETA (Pascual-Marqui, 2002). The spatial resolution of these L2 minimum norm-based approaches is substantially lower than the L1 minimum norm-based solution, such as Fast-VESTAL (Huang et al., 2014a) and standard VESTAL (Huang et al., 2006). Such big spatial resolution difference lies in the different ways in treating sparse source configurations: The L2 minimum norm solutions severely penalize sparse source configurations, whereas the L1 minimum norm solution allows for the formation of sparse source configurations (i.e., with high-resolution solutions).

In summary, using our recently developed high-resolution MEG source imaging technique (i.e., Fast-VESTAL), the present study showed that expressive as well as receptive language areas can be accurately localized during the object-naming task in patients with brain tumors and epilepsies. The expressive language area was localized to Broca's area in the pars opercularis (BA 44) and/or pars triangularis (BA 45), whereas the receptive language area was localized to Wernicke's area in the posterior aspect of the superior temporal gyri in BA 22. The main peak of Wernicke's responses was significantly earlier than that of Broca's responses. One limitation of the present study has been the lack of complete records of surgical conformation, from the patients who underwent surgeries. Such information had not been collected systematically in the past, an area we are currently improving in our clinical practice. In essence, the present study demonstrates that, with the newly established high-resolution source imaging method (i.e., Fast-VESTAL), MEG can serve as an accurate and reliable functional imaging tool for presurgical mapping of language functions in patients with brain tumors and/or epilepsies.

Acknowledgments

This work was supported in part by Merit Review Grants from the Department of Veterans Affairs to M.X. Huang (I01-CX000499, NURC-022-10F, MHBA-010-14F) and R.R. Lee. We also thank the anonymous reviewers for their constructive suggestions that substantially strengthen this study.

Conflict of interest: None of the authors have potential conflicts of interest to be disclosed.

Appendix A. Supplementary data

Supplementary data associated with this article can be found, in the online version, at http://dx.doi.org/10.1016/j.clinph.2016.02.007.

References

Bates E, D'Amico S, Jacobsen T, Szekely A, Andonova E, Devescovi A, Herron D, Lu CC, Pechmann T, Pleh C, Wicha N, Federmeier K, Gerdjikova I, Gutierrez G, Hung D, Hsu J, Iyer G, Kohnert K, Mehotcheva T, Orozco-Figueroa A, Tzeng A, Tzeng O. Timed picture naming in seven languages. Psychon Bull Rev 2003;10:344–80.

Benjamini Y, Hochberg Y. Controlling the false positive rate: a practical and powerful approach to multiple testing. J R Stat Soc Ser B 1995;57:289–300.

Billingsley-Marshall RL, Clear T, Mencl WE, Simos PG, Swank PR, Men D, Sarkari S, Castillo EM, Papanicolaou AC. A comparison of functional MRI and magnetoencephalography for receptive language mapping. J Neurosci Methods 2007;161:306–13.

Bourguignon M, Jousmäki V, Marty B, Wens V, Op de Beeck M, Van Bogaert P, Bogaert P, et al. Comprehensive functional mapping scheme for non-invasive primary sensorimotor cortex mapping. Brain Topogr 2013;26:511–23.

Chen YH, Edgar JC, Huang M, Hunter MA, Epstein E, Howell B, Lu BY, Bustillo J, Miller GA, Canive JM. Frontal and superior temporal auditory processing abnormalities in schizophrenia. Neuroimage Clin 2013;2:695–702.

Cohen D, Schläpfer U, Ahlfors S, Hämäläinen M, Halgren E. New six-layer magnetically-shielded room for MEG. In: Nowak HHJ, Gießler F, editors. Proceedings of the 13th International Conference on Biomagnetism. Jena, Germany: VDE Verlag; 2002. p. 919–21.

Dale AM, Liu AK, Fischl BR, Buckner RL, Belliveau JW, Lewine JD, Halgren E. Dynamic statistical parametric mapping: combining fMRI and MEG for high-resolution imaging of cortical activity. Neuron 2000;26:55–67.

Demonet JF, Price C, Wise R, Frackowiak RS. Differential activation of right and left posterior sylvian regions by semantic and phonological tasks: a positron-emission tomography study in normal human subjects. Neurosci Lett 1994;182:25–8.

Devlin JT, Matthews PM, Rushworth MF. Semantic processing in the left inferior prefrontal cortex: a combined functional magnetic resonance imaging and transcranial magnetic stimulation study. J Cogn Neurosci 2003;15:71–84.

Diwakar M, Harrington DL, Maruta J, Ghajar J, El-Gabalawy F, Muzzatti L, Corbetta M, Huang MX, Lee RR. Filling in the gaps: anticipatory control of eye movements in chronic mild traumatic brain injury. Neuroimage Clin 2015;8:210–23.

Edgar JC, Yeo RA, Gangestad SW, Blake MB, Davis JT, Lewine JD, Canive JM. Reduced auditory M100 asymmetry in schizophrenia and dyslexia: applying a developmental instability approach to assess atypical brain asymmetry. Neuropsychologia 2006;44:289–99.

Edgar JC, Hanlon FM, Huang MX, Weisend MP, Thoma RJ, Carpenter B, Hoechstetter K, Canive JM, Miller GA. Superior temporal gyrus spectral abnormalities in schizophrenia. Psychophysiology 2008;45:812–24.

Gross J, Ioannides AA. Linear transformations of data space in MEG. Phys Med Biol 1999;44:2081–97.

Gross J, Kujala J, Hamalainen M, Timmermann L, Schnitzler A, Salmelin R. Dynamic imaging of coherent sources: Studying neural interactions in the human brain. Proc Natl Acad Sci USA 2001;98:694–9.

Grummich P, Nimsky C, Pauli E, Buchfelder M, Ganslandt O. Combining fMRI and MEG increases the reliability of presurgical language localization: a clinical study on the difference between and congruence of both modalities. Neuroimage 2006;32:1793–803.

Hirata M, Kato A, Taniguchi M, Saitoh Y, Ninomiya H, Ihara A, Kishima H, Oshino S, Baba T, Yorifuji S, Yoshimine T. Determination of language dominance with synthetic aperture magnetometry: comparison with the Wada test. Neuroimage 2004;23:46–53.

Holodny AI, Schulder M, Liu WC, Maldjian JA, Kalnin AJ. Decreased BOLD functional MR activation of the motor and sensory cortices adjacent to a glioblastoma multiforme: implications for image-guided neurosurgery. AJNR Am J Neuroradiol 1999;20:609–12.

Holodny AI, Schulder M, Liu WC, Wolko J, Maldjian JA, Kalnin AJ. The effect of brain tumors on BOLD functional MR imaging activation in the adjacent motor cortex: implications for image-guided neurosurgery. AJNR Am J Neuroradiol 2000;21:1415–22.

Huang MX, Aine C, Davis L, Butman J, Christner R, Weisend M, Stephen J, Meyer J, Silveri J, Herman M, Lee RR. Sources on the anterior and posterior banks of the central sulcus identified from magnetic somatosensory evoked responses using multistart spatio-temporal localization. Hum Brain Mapp 2000;11:59–76.

Huang MX, Edgar JC, Thoma RJ, Hanlon FM, Moses SN, Lee RR, Paulson KM, Weisend MP, Irwin JG, Bustillo JR, Adler LE, Miller GA, Canive JM. Predicting EEG responses using MEG sources in superior temporal gyrus reveals source asynchrony in patients with schizophrenia. Clin Neurophysiol 2003;114:835–50.

Huang MX, Harrington DL, Paulson KM, Weisend MP, Lee RR. Temporal dynamics of ipsilateral and contralateral motor activity during voluntary finger movement. Hum Brain Mapp 2004;23:26–39.

Huang MX, Lee RR, Miller GA, Thoma RJ, Hanlon FM, Paulson KM, Martin K, Harrington DL, Weisend MP, Edgar JC, Canive JM. A parietal-frontal network studied by somatosensory oddball MEG responses, and its cross-modal consistency. Neuroimage 2005;28:99–114.

Huang MX, Dale AM, Song T, Halgren E, Harrington DL, Podgorny I, Canive JM, Lewis S, Lee RR. Vector-based spatial-temporal minimum L1-norm solution for MEG. Neuroimage 2006;31:1025–37.

Huang MX, Song T, Hagler Jr DJ, Podgorny I, Jousmaki V, Cui L, Gaa K, Harrington DL, Dale AM, Lee RR, Elman J, Halgren E. A novel integrated MEG and EEG analysis method for dipolar sources. Neuroimage 2007;37:731–48.

Huang MX, Theilmann RJ, Robb A, Angeles A, Nichols S, Drake A, D'Andrea J, Levy M, Holland M, Song T, Ge S, Hwang E, Yoo K, Cui L, Baker DG, Trauner D, Coimbra R, Lee RR. Integrated imaging approach with MEG and DTI to detect mild traumatic brain injury in military and civilian patients. J Neurotrauma 2009;26:1213–26.

Huang MX, Lee RR, Gaa KM, Song T, Harrington DL, Loh C, Theilmann RJ, Edgar JC, Miller GA, Canive JM, Granholm E. Somatosensory system deficits in schizophrenia revealed by MEG during a median-nerve oddball task. Brain Topogr 2010;23:82–104.

Huang MX, Nichols S, Robb A, Angeles A, Drake A, Holland M, Asmussen S, D'Andrea J, Chun W, Levy M, Cui L, Song T, Baker DG, Hammer P, McLay R, Theilmann RJ, Coimbra R, Diwakar M, Boyd C, Neff J, Liu TT, Webb-Murphy J, Farinpour R, Cheung C, Harrington DL, Heister D, Lee RR. An automatic MEG low-frequency source imaging approach for detecting injuries in mild and moderate TBI patients with blast and non-blast causes. Neuroimage 2012;61:1067–82.

Huang MX, Huang CW, Robb A, Angeles A, Nichols SL, Baker DG, Song T, Harrington DL, Theilmann RJ, Srinivasan R, Heister D, Diwakar M, Canive JM, Edgar JC, Chen YH, Ji Z, Shen M, El-Gabalawy F, Levy M, McLay R, Webb-Murphy J, Liu TT, Drake A, Lee RR. MEG source imaging method using fast L1 minimum-norm and its applications to signals with brain noise and human resting-state source amplitude images. Neuroimage 2014a;84:585–604.

Huang MX, Nichols S, Baker DG, Robb A, Angeles A, Yurgil KA, Drake A, Levy M, Song T, McLay R, Theilmann RJ, Diwakar M, Risbrough VB, Ji Z, Huang CW, Chang DG, Harrington DL, Muzzatti L, Canive JM, Christopher EJ, Chen YH, Lee RR. Single-subject-based whole-brain MEG slow-wave imaging approach for detecting abnormality in patients with mild traumatic brain injury. Neuroimage Clin 2014b;5:109–19.

Huang MX, Yurgil KA, Robb A, Angeles A, Diwakar M, Risbrough VB, Nichols SL, McLay R, Theilmann RJ, Song T, Huang CW, Lee RR, Baker DG. Voxel-wise resting-state MEG source magnitude imaging study reveals neurocircuitry abnormality in active-duty service members and veterans with PTSD. Neuroimage Clin 2014c;5:408–19.

Kober H, Moller M, Nimsky C, Vieth J, Fahlbusch R, Ganslandt O. New approach to localize speech relevant brain areas and hemispheric dominance using spatially filtered magnetoencephalography. Hum Brain Mapp 2001;14:236–50.

Leahy RM, Mosher JC, Spencer ME, Huang MX, Lewine JD. A study of dipole localization accuracy for MEG and EEG using a human skull phantom. Electroencephalogr Clin Neurophysiol 1998;107:159–73.

Misiurski C, Blumstein SE, Rissman J, Berman D. The role of lexical competition and acoustic-phonetic structure in lexical processing: evidence from normal subjects and aphasic patients. Brain Lang 2005;93:64–78.

Mosher JC, Leahy RM, Lewis PS. EEG and MEG: forward solutions for inverse methods. IEEE Trans Biomed Eng 1999;46:245–59.

Mummery CJ, Patterson K, Hodges JR, Price CJ. Functional neuroanatomy of the semantic system: divisible by what? J Cogn Neurosci 1998;10:766–77.

Nakasato N, Kumabe T, Kanno A, Ohtomo S, Mizoi K, Yoshimoto T. Neuromagnetic evaluation of cortical auditory function in patients with temporal lobe tumors. J Neurosurg 1997;86:610–8.

Niranjan A, Laing EJ, Laghari FJ, Richardson RM, Lunsford LD. Preoperative magnetoencephalographic sensory cortex mapping. Stereotact Funct Neurosurg 2013;91:314–22.

Pang EW, Drake JM, Otsubo H, Martineau A, Strantzas S, Cheyne D, Gaetz W. Intraoperative confirmation of hand motor area identified preoperatively by magnetoencephalography. Pediatr Neurosurg 2008;44:313–7.

Pang EW, Wang F, Malone M, Kadis DS, Donner EJ. Localization of Broca's area using verb generation tasks in the MEG: validation against fMRI. Neurosci Lett 2011;490:215–9.

Papanicolaou AC, Simos PG, Breier JI, Zouridakis G, Willmore LJ, Wheless JW, Constantinou JE, Maggio WW, Gormley WB. Magnetoencephalographic mapping of the language-specific cortex. J Neurosurg 1999;90:85–93.

Papanicolaou AC, Simos PG, Castillo EM, Breier JI, Sarkari S, Pataraia E, Billingsley RL, Buchanan S, Wheless J, Maggio V, Maggio WW. Magnetoencephalography: a noninvasive alternative to the Wada procedure. J Neurosurg 2004;100:867–76.

Papanicolaou AC, Simos PG, Castillo EM. MEG localization of language-specific cortex utilizing MR-FOCUSS. Neurology 2005;64:765.

Papanicolaou AC, Pazo-Alvarez P, Castillo EM, Billingsley-Marshall RL, Breier JI, Swank PR, Buchanan S, McManis M, Clear T, Passaro AD. Functional neuroimaging with MEG: normative language profiles. Neuroimage 2006;33:326–42.

Pascual-Marqui RD. Standardized low-resolution brain electromagnetic tomography (sLORETA): technical details. Methods Find Exp Clin Pharmacol 2002;24(Suppl. D):5–12.

Price CJ. The anatomy of language: contributions from functional neuroimaging. J Anat 2000;197(Pt 3):335–59.

Price CJ, Moore CJ, Humphreys GW, Wise RJ. Segregating semantic from phonological processes during reading. J Cogn Neurosci 1997;9:727–33.

Rezaie R, Narayana S, Schiller K, Birg L, Wheless JW, Boop FA, Papanicolaou AC. Assessment of hemispheric dominance for receptive language in pediatric patients under sedation using magnetoencephalography. Front Hum Neurosci 2014;8:657.

Robb SA, Nichols S, Drake A, Angeles A, Diwakar M, Song T, Lee RR, Huang MX. Magnetoencephalography slow-wave detection in patients with mild traumatic brain injury and ongoing symptoms correlated with long-term neuropsychological outcome. J Neurotrauma 2015;32:1510–21.

Robinson SE, Vrba J. Functional neuroimaging by syntheticaperture magnetometry (SAM). In: Yoshimoto T, Kotani M, Kuriki S, Karibe H, Nakasato N, editors. Recent Advances in Biomagnetism. Sendai, Japan: Tohoku University Press; 1999. p. 302–5.

Roux FE, Boulanouar K, Lotterie JA, Mejdoubi M, LeSage JP, Berry I. Language functional magnetic resonance imaging in preoperative assessment of language areas: correlation with direct cortical stimulation. Neurosurgery 2003;52:1335–45.

Sakai KL, Noguchi Y, Takeuchi T, Watanabe E. Selective priming of syntactic processing by event-related transcranial magnetic stimulation of Broca's area. Neuron 2002;35:1177–82.

Salmelin R, Hari R, Lounasmaa OV, Sams M. Dynamics of brain activation during picture naming. Nature 1994;368:463–5.

Schiffbauer H, Ferrari P, Rowley HA, Berger MS, Roberts TP. Functional activity within brain tumors: a magnetic source imaging study. Neurosurgery 2001;49:1313–20.

Schiffbauer H, Berger MS, Ferrari P, Freudenstein D, Rowley HA, Roberts TP. Preoperative magnetic source imaging for brain tumor surgery: a quantitative comparison with intraoperative sensory and motor mapping. Neurosurg Focus 2003;15:E7.

Schreiber A, Hubbe U, Ziyeh S, Hennig J. The influence of gliomas and nonglial space-occupying lesions on blood-oxygen-level-dependent contrast enhancement. AJNR Am J Neuroradiol 2000;21:1055–63.

Sekihara K, Nagarajan SS, Poeppel D, Marantz A, Miyashita Y. Reconstructing spatio-temporal activities of neural sources using an MEG vector beamformer technique. IEEE Trans Biomed Eng 2001;48:760–71.

Silkes JP, Rogers MA. Masked priming effects in aphasia: evidence of altered automatic spreading activation. J Speech Lang Hear Res 2012;55:1613–25.

Song T, Gaa K, Cui L, Feffer L, Lee RR, Huang M. Evaluation of signal space separation via simulation. Med Biol Eng Comput 2008;46:923–32.

Stoeckel C, Gough PM, Watkins KE, Devlin JT. Supramarginal gyrus involvement in visual word recognition. Cortex 2009;45:1091–6.

Szekely A, D'Amico S, Devescovi A, Federmeier K, Herron D, Iyer G, Jacobsen T, Arevalo AL, Vargha A, Bates E. Timed action and object naming. Cortex 2005;41:7–25.

Tadel F, Baillet S, Mosher JC, Pantazis D, Leahy RM. Brainstorm: a user-friendly application for MEG/EEG analysis. Comput Intell Neurosci 2011;2011:879716.

Taulu S, Simola J. Spatiotemporal signal space separation method for rejecting nearby interference in MEG measurements. Phys Med Biol 2006;51:1759–68.

Taulu S, Kajola M, Simola J. Suppression of interference and artifacts by the signal space separation method. Brain Topogr 2004a;16:269–75.

Taulu S, Simola J, Kajola M. MEG recordings of DC fields using the signal space separation method (SSS). Neurol Clin Neurophysiol 2004b;2004:35.

Uutela K, Hamalainen M, Somersalo E. Visualization of magnetoencephalographic data using minimum current estimates. Neuroimage 1999;10:173–80.

Van Veen BD, Van DW, Yuchtman M, Suzuki A. Localization of brain electrical activity via linearly constrained minimum variance spatial filtering. IEEE Trans Biomed Eng 1997;44:867–80.

Wada J, Rasmussen T. Intracarotid injection of sodium amytal for the lateralization of cerebral speech dominance: experimental and clinical observations. J Neurosurg 1960;17:266–82.